




SEPTEMBER 13 2023

Willis couplings in continuously varying cross-sectional area duct

A. Krpenský  ; M. Bednařík  ; J-P. Groby 



J. Acoust. Soc. Am. 154, 1660–1666 (2023)

<https://doi.org/10.1121/10.0020849>



View
Online



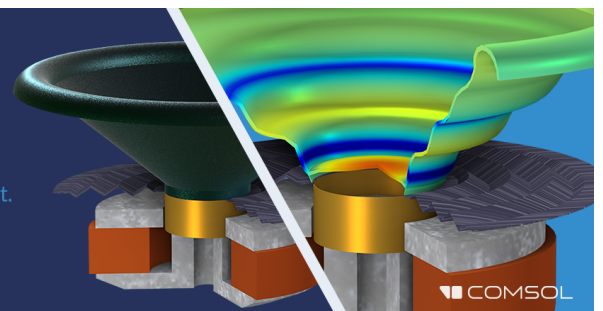
Export
Citation

CrossMark

Take the Lead in Acoustics

The ability to account for coupled physics phenomena lets you predict, optimize, and virtually test a design under real-world conditions – even before a first prototype is built.

» Learn more about COMSOL Multiphysics®



Willis couplings in continuously varying cross-sectional area duct

A. Krpenský,¹  M. Bednařík,¹  and J.-P. Groby^{2,a)} 

¹Faculty of Electrical Engineering, Department of Physics, Czech Technical University in Prague, Technická 2, 166 27 Prague 6, Czech Republic

²Laboratoire d'Acoustique de l'Université du Mans, Unité Mixte de Recherche 6613, Institut d'Acoustique - Graduate School, Centre National de la Recherche Scientifique, Le Mans Université, France

ABSTRACT:

Acoustic wave propagation in a one-dimensional periodic and asymmetric duct is studied theoretically and numerically to derive the effective properties. Closed form expressions for these effective properties, including the asymmetric Willis coupling, are derived through truncation of the Peano–Baker series expansion of the matricant (which links the state vectors at the two sides of the unit-cell) and Padé's approximation of the matrix exponential. The results of the first-order and second-order homogenization (with Willis coupling) procedures are compared with the numerical results. The second-order homogenization procedure provides scattering coefficients that are valid over a much larger frequency range than the usual first-order procedure. The frequency well below which the effective description is valid is compared with the lower bound of the first Bragg bandgap when the profile is approximated by a two-step function of identical indicator function, i.e., two different cross-sectional areas over the same length. This validity limit is then questioned, particularly with a focus on impedance modeling. This article attempts to facilitate the engineering use of Willis materials. © 2023 Acoustical Society of America. <https://doi.org/10.1121/10.0020849>

(Received 3 April 2023; revised 4 August 2023; accepted 20 August 2023; published online 13 September 2023)

[Editor: Yong Li]

Pages: 1660–1666

I. INTRODUCTION

Since the seminal work of Willis in the 1980s,¹ the eponymous materials have received an increasing attention. This increasing attention has even been exponential since their experimental evidence or demonstration.^{2–4} The Willis coupling parameters couple the potential and kinetic energy in the acoustic conservation relations; therefore, enhancing the ability to control waves in metamaterials compared to other materials that do not exhibit such coupling. These parameters have thus been employed to design and analyze \mathcal{PT} symmetric,⁵ wave front shaping,⁶ or non-reciprocal^{7–9} systems. Most of the works to date have focused on the physical origins,¹⁰ calculation,^{11–13} and enhancement¹⁴ of Willis coupling, but only a few have focused on deriving a closed form of these parameters¹⁵ to ease Willis material engineering use. Effectively, various systems are asymmetric and can thus be modeled as Willis materials. In this article, we will focus on a one-dimensional (1D) periodic system, the properties of which vary continuously in a periodic manner.

This system simply consists of a duct, the radius of which varies continuously and periodically, leading to an asymmetric profile. The acoustic wave propagation of such a system has been extensively studied in the past, mostly for two purposes: the acoustic wave propagation in horns^{16,17} and in corrugated ducts in the absence¹⁸ or in the presence¹⁹ of flow. The propagation of plane acoustic waves in ducts,

the cross-sectional area of which varies in space, is generally based on the Webster equation. This equation is commonly used to analyze and design mufflers, resonators, and other types of acoustic filters for noise control applications,^{20,21} but also in the analysis of musical instruments, such as flutes and organ pipes, where the geometry of the instrument affects the resonance frequencies and the sound quality.²² An accurate, or at least a reasonably close, analytical solution for the Webster equation is thus crucial to study the behavior of sound waves in such systems. Several papers have been dedicated to solving this equation.^{23–26} Although an approximate analytical solution accounting for viscothermal losses has been proposed,²⁷ these losses that occur at the duct boundaries are often neglected. To our knowledge, any of the former articles were focused on deriving the effective properties in such problems in the presence of viscothermal losses and when the corrugation profile is asymmetric.

Inspired by Refs. 9, 15, and 28, the closed form expressions of the effective properties, including the asymmetric Willis coupling, describing the acoustic wave propagation in a duct (the radius of which varies periodically and continuously) are derived and analyzed. A related article was published on elasticity,¹² in which the procedure was different and validated on a two-layer laminate under SH polarization.

The article is organized as follows. In Sec. II, the equations describing the acoustic wave propagation in the duct of continuously varying radius are reminded. The procedure to derive the effective properties, based on the first-order Padé's approximation of the matrix exponential and

^{a)}Email: Jean-Philippe.Groby@univ-lemans.fr

Peano–Baker series expansion of the matricant, is described and applied to our problem in Sec. III. Results in two specific cases, i.e., one where the profile leads to narrow duct portion of short period and the other where the profile leads to wider duct of longer period, are discussed in Sec. IV. In particular, the dispersion introduced by the radius profile is analyzed in view of homogenization limit.

II. GENERAL STATEMENT

We consider the 1D acoustic wave propagation in a d -periodic duct of a continuously varying circular cross-sectional area $S(x) = \pi r(x)^2$ as depicted in Fig. 1. Assuming an implicit time dependence $e^{-i\omega t}$, pressure $p(x)$, and flow $\mathcal{V}(x) = S(x)V(x)$, where $V(x)$ is the particle velocity, satisfy the following first-order equations

$$\begin{cases} i\omega\tilde{\rho}(x)\mathcal{V} = \frac{\partial p}{\partial x}, \\ i\omega\tilde{C}(x)p = \frac{\partial \mathcal{V}}{\partial x}, \end{cases} \quad (1)$$

where $\tilde{\rho}(x) = \rho(x)/S(x)$ and $\tilde{C}(x) = C(x)S(x)$ are, respectively, the reduced density and compressibility (inverse of

the bulk modulus, $\tilde{C} = 1/\tilde{K}$). This system is usually cast in the matrix form

$$\frac{\partial}{\partial x} \mathbf{W} = \begin{bmatrix} 0 & i\omega\tilde{\rho}(x) \\ i\omega\tilde{C}(x) & 0 \end{bmatrix} \mathbf{W} = \mathbf{A}(x)\mathbf{W}, \quad (2)$$

where $\mathbf{W} = \langle p, \mathcal{V} \rangle^T$ is the state vector and $\mathbf{A}(x)$ is the propagation matrix. The latter matrix \mathbf{A} depends on x and does not commute with itself for different values of x , i.e., $\mathbf{A}(x)\mathbf{A}(x') - \mathbf{A}(x')\mathbf{A}(x) \neq 0$ when $x' \neq x$. The solution of the system represented by Eq. (2), which relates the state vectors at both sides of the unit-cell via $\mathbf{W}(d) = \mathbf{M}_d\mathbf{W}(0)$, also involves a matricant \mathbf{M}_d that takes the form of a Peano–Baker series expansion

$$\mathbf{M}_d = \mathbf{Id} + \int_0^d \mathbf{A}(x)dx + \int_0^d \mathbf{A}(x) \left(\int_0^x \mathbf{A}(\zeta)d\zeta \right) dx + \dots, \quad (3)$$

which is usually evaluated iteratively. Each iteration corresponds to an increase in the order of the Taylor expansion. Of particular interest is the second-order iteration that reads as

$$\mathbf{M}_d^{(2)} = \begin{bmatrix} 1 - \omega^2 \int_0^d \tilde{\rho}(x) \int_0^x \tilde{C}(\zeta) d\zeta dx & i\omega\bar{\rho}d \\ i\omega\bar{C}d & 1 - \omega^2 \int_0^d \tilde{C}(x) \int_0^x \tilde{\rho}(\zeta) d\zeta dx \end{bmatrix} + \mathcal{O}(\bar{k}d)^3, \quad (4)$$

where $\bar{\rho} = \int_0^d \tilde{\rho}(x) dx/d$ and $\bar{C} = \int_0^d \tilde{C}(x) dx/d$ are the mean values of $\tilde{\rho}$ and \tilde{C} , and $\bar{k} = \omega\sqrt{\bar{\rho}\bar{C}}$.

III. DERIVATION OF THE EFFECTIVE PROPERTIES

We assume a d -periodic 1D reciprocal system of respective propagation matrix \mathbf{A}_e . The state vectors at both sides of the unit-cell are related via $\mathbf{W}(d) = \exp(\mathbf{A}_e d)\mathbf{W}(0) = \mathbf{T}\mathbf{W}(0)$, with \mathbf{T} the transfer matrix of respective elements t_{ij} , $(i, j) \in (1, 2)$. Following Ref. 15, the propagation matrix is correctly approximated by the inversion of the first-order Padé’s approximation of the transfer matrix (i.e., the matrix exponential)

$$\begin{aligned} \mathbf{A}_e &\approx \frac{2}{d}(\mathbf{T} + \mathbf{Id})^{-1}(\mathbf{T} - \mathbf{Id}) \\ &\approx \frac{2}{d} \frac{1}{2 + t_{11} + t_{22}} \begin{bmatrix} t_{11} - t_{22} & 2t_{12} \\ 2t_{21} & t_{22} - t_{11} \end{bmatrix}, \end{aligned} \quad (5)$$

which directly provides the elements of a reciprocal Willis material

$$\mathbf{A}_e = i\omega \begin{bmatrix} \chi_e^a & \rho_e \\ C_e & -\chi_e^a \end{bmatrix}, \quad (6)$$

where ρ_e is the effective density, C_e is the effective compressibility, and χ_e^a is the even Willis coupling related to the

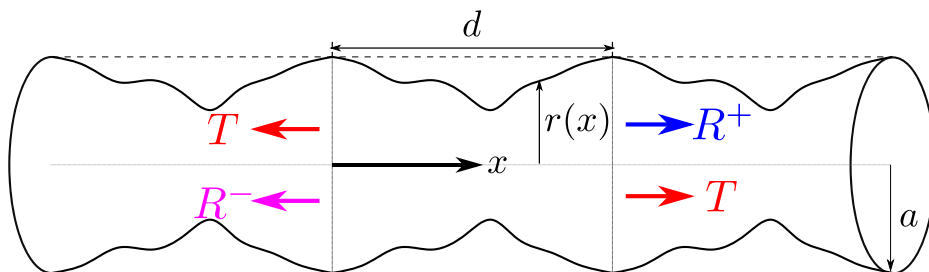


FIG. 1. (Color online) Sketch of the configuration and representation of the scattering problem.

possible asymmetry of the unit-cell. Note that the reciprocal feature of the system, i.e., $\det(\mathbf{T}) = 1$ has been accounted for in Eq. (5). Checking this property can be employed as a validation step (see Appendix A).

Introducing the matricant elements in Eq. (5) leads to

$$\rho_e = \bar{\rho}, \quad C_e = \bar{C},$$

and

$$\chi_e^a = \frac{i\omega}{2d} \left(\int_0^d \tilde{\rho}(x) \int_0^x \tilde{C}(\zeta) d\zeta dx - \int_0^d \tilde{C}(x) \int_0^x \tilde{\rho}(\zeta) d\zeta dx \right). \quad (7)$$

The effective density and compressibility are $\mathcal{O}(\omega)$, while χ_e^a is exhibited at the next order and is thus $\mathcal{O}(\omega)^2$. The effective density and compressibility are classical results from the first-order homogenization. Quantities evaluated according to the first-order homogenization are hereafter referred to as sub-index H . When the profile is symmetric, i.e., $r(x) = r(d - x)$, $\forall x \in [0, d/2]$, χ_e^a vanishes (see the Appendix B) and thus, the effective density and compressibility become valid at the second order. In other words, the first-order homogenization results become valid at the second order when the profile is symmetric. When the profile is piecewise constant, the effective properties,

including the Willis coupling, fall back on the formulas derived in Ref. 28. In addition, the Willis coupling vanishes at low frequency because an asymmetric structure falls back to symmetric at low frequency. The asymmetric Willis coupling is effectively a linear function of the frequency (in the absence of losses) because it appears at the second order. In the absence of losses, χ_e^a is purely imaginary.

IV. RESULTS AND DISCUSSION

We consider a duct, the maximum radius of which is $a = 1.5$ cm, such that the profile $r(x)$ consists of a reduction of this radius. Only plane waves are also propagating below the cut-on frequency of the first mode in a duct of radius a , which is frequencies below ≈ 6100 Hz. Viscothermal losses are accounted for via the Stinson's formula,²⁹ which are addressed in Appendix C. The structuration of the duct geometry introduced by the periodic radial profile $r(x)$ induces dispersion of the waves traveling in the duct. To get a grip on it, the dispersion relation of the acoustic waves in a periodic duct composed of two different cross-sectional areas, S_{max} associated with a radius a and \tilde{S} corresponding to a radius \tilde{r} , of the same length, i.e., $d/2$, is considered. This dispersion relation turns out to be that of a periodic 1D Su-Schrieffer-Heeger model,³⁰ where the coupling coefficients are simply given by the ratios of the two different cross-sectional areas.³¹ This relation reads as

$$\cos(kd/2) = \pm \sqrt{\left(\left(\frac{S_{max}}{S_{max} + \tilde{S}} \right)^2 + \left(\frac{\tilde{S}}{S_{max} + \tilde{S}} \right)^2 + \frac{2S_{max}\tilde{S}}{(S_{max} + \tilde{S})^2} \cos(k_e d) \right)}, \quad (8)$$

where k_e is the effective wavenumber in the presence of the periodic structuration and k is the wave number in the straight duct. When $k_e d = \pi$, the frequency of the lower bound of the first Bragg bandgap can be calculated in the absence of losses. This frequency, $f_{\tilde{r}}^B$, is supposed to provide a good approximation of the quantity well below which the effective models are valid. The question that naturally arises becomes: which value of \tilde{r} (or \tilde{S}) should be considered? We thus consider two limit cases: the first one where kd is small but $r(x)$ leads to a narrow duct portion and the second one where kd is larger and $r(x)$ leads to a wider duct cross-sectional area on average.

Figures 2(a) and 2(b) depict the two continuous profiles considered, the equations of which are provided in Appendix D. In the first case, $d = 2$ cm and the profile has a maximum reduction of the duct radius of 90%. In the second case, $d = 6$ cm and the profile has a maximum reduction of the duct radius of 50% and much less on average. These two profiles are discretized in 301 segments which are used to

evaluate the integrals (trapezoidal rule) in the effective parameter closed form expressions [Eq. (7)]. Instead of iteratively evaluating Eq. (3) to calculate the matricant, we evaluate the total transfer matrix that links the state vectors at both sides of the unit-cell, by multiplying the transfer matrices of each segment T_j , i.e., $T_{tot} = \prod_{j=1}^{301} T_j$. This solution is then considered as the reference solution, from which the effective properties can be numerically evaluated^{12,15} via $A_n = \log(T_{tot})/d$ (see also Appendix E). The corresponding effective properties are referred to as the sub-index n . Figures 2(c)–2(f) depict the dispersion relation (real and imaginary parts of the wavenumber) of the acoustic waves for both profiles. The lower bound of the Bragg bandgap is numerically evaluated around 2300 Hz in both cases. Either $\tilde{r} = \min(r(x))$ (the minimum radius over a period) or $\tilde{r} = 2\bar{r} - a$ (the radius that produces the same area reduction as that produced by the profile) are considered to evaluate $f_{\tilde{r}}^B$. In the first case, $f_{\min(r(x))}^B \approx 1100$ Hz and $f_{2\bar{r}-a}^B \approx 4500$ Hz, while in the second case,

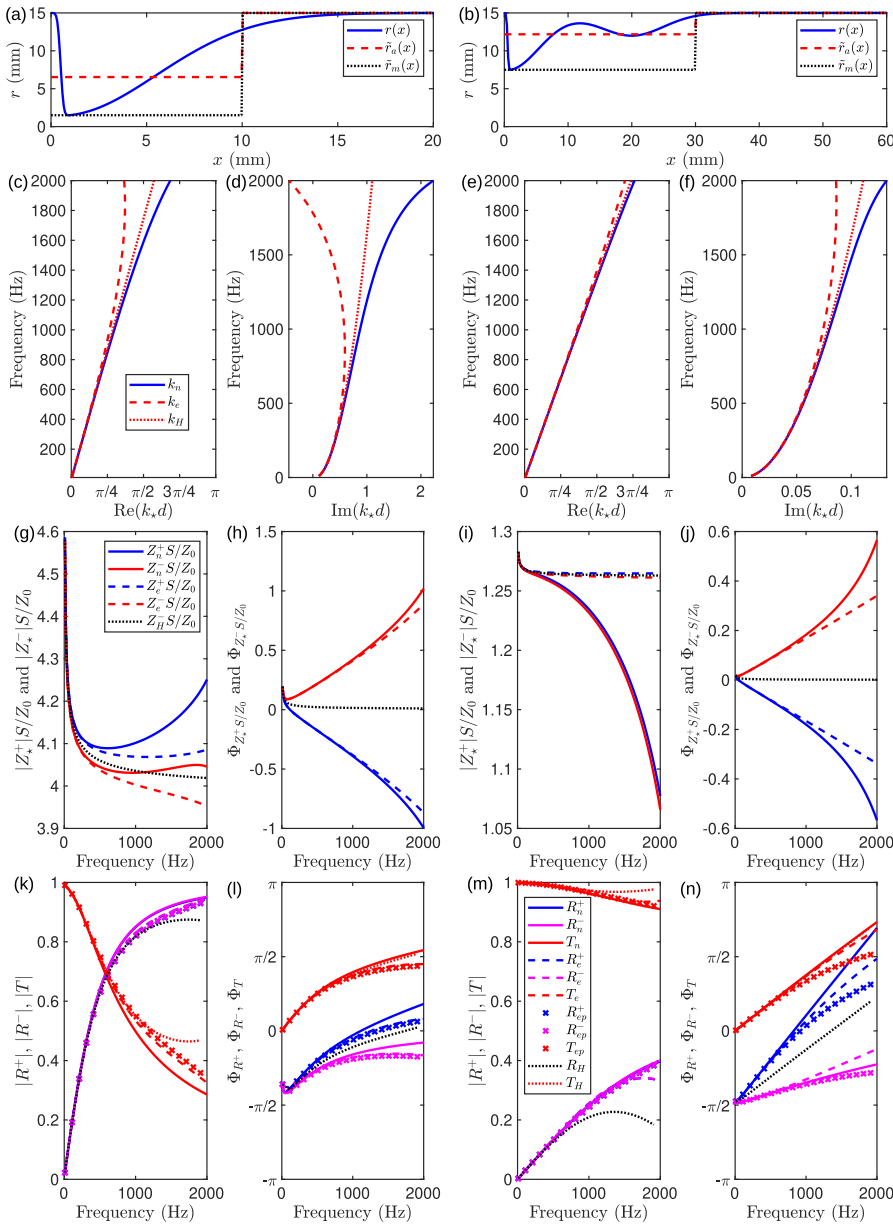


FIG. 2. (Color online) Continuous profiles in the (a) first and (b) second cases (blue curve) as well as the two approximations in two equal portions of different sectional areas with \tilde{r}_a (dashed red curve) and with \tilde{r}_m (dotted black curve). (c) and (e) Real and (d) and (f) imaginary parts of the wavenumber–dispersion relation—in the first and second cases, respectively. (g) and (i) Modulus and (d) and (f) phase of the normalized impedances $Z^\pm S/Z_0$. (g) and (i) Modulus and (d) and (f) phase of the scattering coefficients, i.e., R^+ , R^- , and T . (c)–(f) Results as calculated numerically (continuous curves), with the first-order homogenization (dotted curves), and with the second-order homogenization (dashed curves) procedures. (k)–(n) The markers refer to the scattering coefficients as calculated with the first-order Padé’s approximation of $\expm(A_e d)$.

$f_{\min(r(x))}^B \approx 1700$ Hz and $f_{2\bar{r}-a}^B \approx 2500$ Hz. Although this frequency is better approximated in the second case than in the first case, $f_{\min(r(x))}^B \approx 1100$ Hz and $f_{2\bar{r}-a}^B \approx 2500$ Hz seem to be appropriate for the first and second cases, respectively, in view of the homogenization limit. In terms of rule, if $2\bar{r} - a > a/2$, $f_{2\bar{r}-a}^B$ is appropriate and if $2\bar{r} - a < a/2$, $f_{\min(r(x))}^B$ is appropriate. Nevertheless, speaking in terms of percentage of k_{ed} does not seem to be representative when asymmetric structures are considered because the main difference between first and second homogenization is not in $k_H = \omega\sqrt{\rho_e C_e}$ instead of $k_e = \omega\sqrt{\rho_e C_e + \chi_e^2}$ but rather in $Z_H = \sqrt{\rho_e/C_e}$ instead of $Z_e^\pm = \rho_e/(\sqrt{\rho_e C_e + \chi_e^2} \mp \chi)$. The wavenumber k_n is even better approximated by k_H than it is by k_e over the considered frequency range, as can be seen in Figs. 2(c)–2(f). Please note that the range of $\text{Re}(k_e d)$ over which the dispersion relationships are represented is large

and far exceeds the range of validity of the usual homogenization procedures. The two impedances Z_n^\pm are better approximated by Z_e^\pm than they are by Z_H and in particular, their phases [see Figs. 2(g)–2(j)]. Please note that the dynamics of the impedance modulus in the second case [Fig. 2(i)] is different from that in the first case [Fig. 2(g)]. The ratio between the wavelength and the period is thus not the only limit in terms of homogenization, because it only relies on the effective wavenumber and the impedance has also to be accounted for. This is clearly visible on the scattering coefficients by a single unit-cell depicted in Figs. 2(k)–2(n). In both cases, the scattering coefficients calculated via the second-order homogenization, that is, when the Willis coupling is accounted for, is accurate over a wider range of frequencies than those calculated via the first-order homogenization. Although this is an obvious result, it is worth noting. The asymmetry of the radius profiles are more

visible on the phases of the reflection coefficients than on their moduli. These phase differences are clearly exhibited when Willis coupling is accounted for via Z_e^\pm [see Figs. 2(h) and 2(j)]. The phase of the reflection coefficient as calculated with the first-order homogenization stands between those as calculated with the Willis coupling. At low frequencies, the phases are equal because an asymmetric structure falls back to symmetric. When the frequency increases, the phases start to differentiate. The results of the first-order homogenization results fail when the phase difference between the two reflection coefficients become too large, while the results of the second-order homogenization are still satisfactory. The second-order homogenization fails for both transmission and reflection coefficients when the phase of the reflection coefficients are not correctly modeled anymore. Please note that the scattering coefficients of a single unit-cell as calculated with the first-order Padé's approximation of the function $\expm(A_e d)$ is in good agreement with the numerically calculated scattering coefficients. This means that the main source of error in the derivation of the effective properties yields in the truncation of the Peano–Baker series to evaluate the matricant at the second

iteration (second-order Taylor expansion). Please also note that for longer structures, i.e., more than a single unit-cell, the matrix exponential is mandatory to evaluate the scattering coefficients. Finally, the impact of the error on k_e and Z_e^\pm can be tempered in the case of longer structures. Indeed, the error on k_e can have a greater impact in this case, as the wave propagates over a greater distance in the material.

Figures 3(a)–3(l) depict the normalized effective properties as evaluated numerically (blue continuous curves) and from their closed form expressions (red dashed curves) given in Eq. (7) for both profiles. Closed form expressions are in excellent agreement with the numerical results, although they deviate when the frequency increases. As pointed out in the previous paragraph, these effective properties are valid over a shorter frequency range in the first case, which is when the profile leads to a narrow duct portion, than in the second case, which is when the period is longer, and the duct is wider. Whatever the case, the Willis coupling cannot be neglected in relation to the other effective parameters at high frequency. The Willis coupling is almost purely imaginary which is in accordance with Eq. (7). Compared to the other normalized effective properties, the Willis coupling clearly

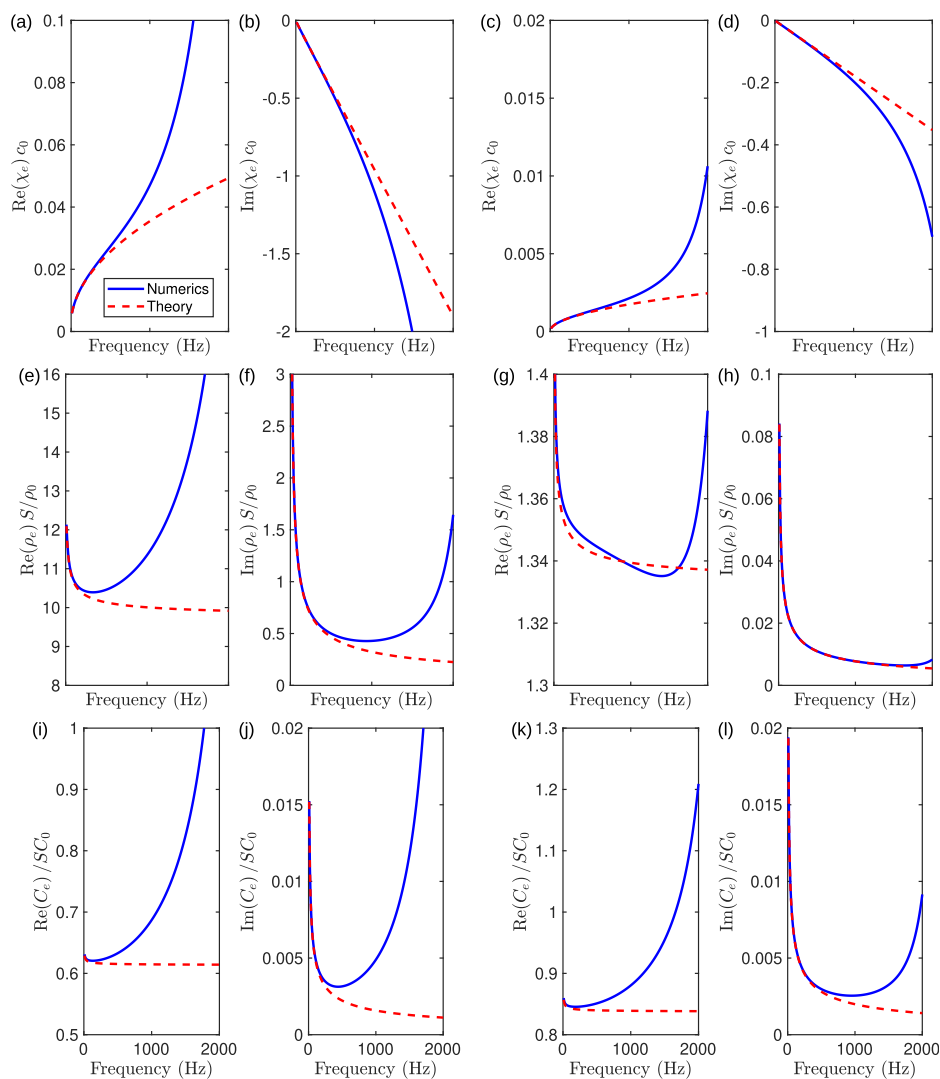


FIG. 3. (Color online) (a) and (c) Real and (b) and (d) imaginary parts of the normalized asymmetric Willis coupling. (e) and (g) Real and (f) and (h) imaginary parts of the normalized effective density. (i) and (k) Real and (j) and (l) imaginary parts of the normalized effective compressibility. Numerical results are depicted in blue continuous curves and closed form expressions of the coefficients are depicted in red dashed curves.

cannot be neglected, which emphasizes the need to use a second-order homogenization procedure.

V. CONCLUSION

The effective properties describing the acoustic wave propagation in a duct, the radius of which varies continuously and periodically and leads to an asymmetric over the period, are derived with the help of the first-order Padé’s approximation of the matrix exponential function and truncation of the Peano–Baker series. Each iteration corresponds to an increase in the order of the Taylor expansion. The first-order (classical) homogenization results are recovered using the first iteration to evaluate the matricant, while the second-order homogenization, derived using the second iteration to evaluate the matricant, features the Willis coupling as an additional parameter. The lowest bound of the first Bragg bandgap, when the unit-cell radius profile is approximated by a two-step function of identical indicator function, is considered to assess the frequency well below which the effective models are valid. The radial structuration actually induces wave dispersion. It turns out that the validity of the effective Willis material derived to model this asymmetric periodic duct not only relies on a percentage of k_{ed} , but also on the impedance modeling. Effectively, the asymmetric Willis coupling that is exhibited at the second order impacts the effective wavenumber but also makes the impedance of the wave propagating in the positive or in the negative directions different as the unit-cell is asymmetric. The modeling of these two impedances has also to be accounted for to derive the real and practical validity limit of the scattering coefficients calculated with the effective properties. Wavenumbers, impedances, effective properties, and scattering coefficients, as calculated with the second-order homogenization procedure, are found in good agreement with the numerical results calculated with the standard transfer matrix method, thus validating the proposed method. This article paves the way for the modeling of more complicated ducts with periodic asymmetric radial structuration, like acoustic black holes, possibly in the presence of flow. It also questions the validity limits of the effective properties.

ACKNOWLEDGMENTS

This work was supported by the Grant Agency of the Czech Republic Grant No. 22-33896S. J.-P.G. is thankful for the financial support of the Metaroom Project No. ANR-18-CE08-0021 which is co-funded by A.N.R. and R.C.G.

APPENDIX A: VERIFYING THAT THE MATRICANT IS UNITARY AT THE SECOND ORDER

The determinant of the matrix Eq. (4) reads as

$$\begin{aligned} \det(\mathbf{M}_d^{(2)}) &= 1 + \omega^2 \left(\bar{C}\bar{\rho} - \int_0^d \tilde{C}(x) \int_0^x \tilde{\rho}(\zeta) d\zeta dx \right. \\ &\quad \left. - \int_0^d \tilde{\rho}(x) \int_0^x \tilde{C}(\zeta) d\zeta dx \right) + \mathcal{O}(\bar{k}d)^3 \\ &= 1 + \mathcal{O}(\bar{k}d)^3. \end{aligned} \tag{A1}$$

Note that Eq. (A1) vanishes because both functions $\tilde{\rho}(x)$ and $\tilde{C}(x)$ are zero for $x < 0$ and integration by part formula.

APPENDIX B: CANCELLATION OF THE WILLIS COUPLING IN THE CASE OF A SYMMETRIC PROFILE

Equation (7) can be further expanded as follows:

$$\begin{aligned} \chi_e^a &= \frac{i\omega}{2d} \left(\bar{\rho} \int_0^{d/2} \tilde{C}(x) dx - \bar{C} \int_0^{d/2} \tilde{\rho}(x) dx \right. \\ &\quad \left. + \int_0^d \tilde{C}(x) \int_{d/2}^x \tilde{\rho}(\zeta) d\zeta dx \right. \\ &\quad \left. - \int_0^d \tilde{\rho}(x) \int_{d/2}^x \tilde{C}(\zeta) d\zeta dx \right). \end{aligned} \tag{B1}$$

When the profile is symmetric, i.e., $r(x)$ is symmetric with respect to $d/2$, the first two terms in Eq. (B1) cancel (since $\int_0^{d/2} \tilde{\rho}(x) dx = \bar{\rho}d/2$ and $\int_0^{d/2} \tilde{C}(x) dx = \bar{C}d/2$) and the last two terms vanish since they represent an integration over $[0; d/2]$ of a multiple of a symmetric and an antisymmetric function with respect to $d/2$.

APPENDIX C: ACCOUNTING FOR THE VISCO-THERMAL LOSSES

Circular cross-sectional ducts are considered throughout this article. The boundaries give rise to visco-thermal losses from viscous and thermal skin depths. Assuming that only plane waves propagate in a circular cross-sectional duct of radius r , the effective complex and frequency dependent density and compressibility read as²⁹

$$\begin{aligned} \rho &= \rho_0 \left(1 - \frac{2}{r\sqrt{i\omega\rho_0/\eta}} \frac{J_1(r\sqrt{i\omega\rho_0/\eta})}{J_0(r\sqrt{i\omega\rho_0/\eta})} \right)^{-1}, \\ C &= \left(1 + \frac{2(\gamma - 1)}{r\sqrt{iPr\omega\rho_0/\eta}} \frac{J_1(r\sqrt{iPr\omega\rho_0/\eta})}{J_0(r\sqrt{iPr\omega\rho_0/\eta})} \right) / \gamma P_0, \end{aligned} \tag{C1}$$

where ρ_0 , γ , η , and Pr are, respectively, the density, specific heat ratio, dynamic density, and Prandtl number of the saturating fluid, and P_0 is the atmospheric pressure. The reduced density and bulk modulus can then be evaluated by $\tilde{\rho}(x) = \rho(x)/S(x)$ and $\tilde{C}(x) = C(x)S(x)$, with $S(x) = \pi r(x)^2$ for each value of $r(x)$.

APPENDIX D: EQUATIONS OF THE TWO PROFILES

The equations of the two profiles considered are provided below. Both are generated via asymmetric Gaussian functions

$$\mathcal{G}(x) = \frac{1}{\sqrt{2\pi}} \exp\left(-\frac{(x/\sigma - \zeta)^2}{2}\right) \left(1 + \operatorname{erf}\left(\alpha \frac{x/\sigma - \zeta}{\sqrt{2}}\right)\right), \tag{D1}$$

with $\operatorname{erf}(x)$ being the error function and σ , ζ , and α being the constant values.

The period d is 2 cm in the first case and the profile is

$$r(x) = a - 0.9a \frac{\mathcal{G}(x)}{\max(\mathcal{G}(x))}, \quad (\text{D2})$$

with $\alpha = 40$, $\zeta = 0.1$, and $\sigma = 5 \times 10^{-3}$, and $\max(f(x))$ is the maximum value of $f(x)$, $x \in [0, d]$. The period d is 6 cm in the second case and the profile is

$$r(x) = a - 0.5a \frac{\mathcal{G}(x)}{\max(\mathcal{G}(x))} - 0.2a \frac{\mathcal{G}^\dagger(x)}{\max(\mathcal{G}^\dagger(x))}, \quad (\text{D3})$$

with $\alpha = \alpha^\dagger = 40$, $\zeta = 0.1$, and $\sigma = 5 \times 10^{-3}$, and $\zeta^\dagger = 0.2$, and $\sigma^\dagger = 5 \times 10^{-2}$.

APPENDIX E: NUMERICAL EVALUATION OF THE EFFECTIVE PROPERTIES

Let us assume that the state vectors at both sides of the unit-cell of length d are linked by the total transfer matrix \mathbf{T}_{tot} . The effective properties can be numerically evaluated via

$$\begin{aligned} \mathbf{A}_n &= \log m(\mathbf{T}_{\text{tot}}) / d \\ &= i\omega \begin{bmatrix} \chi_n^a & \rho_n \\ C_n & -\chi_n^a \end{bmatrix} \\ &= \frac{1}{\sqrt{2}} \begin{bmatrix} Z_n^+ & -Z_n^- \\ 1 & 1 \end{bmatrix} \begin{bmatrix} ik_n & 0 \\ 0 & -ik_n \end{bmatrix} \frac{1}{\sqrt{2}} \begin{bmatrix} 1/Z_n^+ & -1 \\ 1/Z_n^- & 1 \end{bmatrix}. \end{aligned} \quad (\text{E1})$$

The impedances Z_n^\pm and wavenumber k_n can simply be calculated from the diagonalization of \mathbf{A}_e . This procedure turns out to be a numerical version of the procedure derived in Ref. 12.

¹J. Willis, "Variational principles for dynamic problems for inhomogeneous elastic media," *Wave Motion* **3**, 1–11 (1981).
²S. Koo, C. Cho, J. Jeong, and N. Park, "Acoustic omni meta-atom for decoupled access to all octants of a wave parameter space," *Nat. Commun.* **7**, 13012 (2016).
³M. B. Muhlestein, C. F. Sieck, P. S. Wilson, and M. R. Haberman, "Experimental evidence of Willis coupling in a one-dimensional effective material element," *Nat. Commun.* **8**, 15625 (2017).
⁴Y. Liu, Z. Liang, J. Zhu, L. Xia, O. Mondain-Monval, T. Brunet, A. Alù, and J. Li, "Willis metamaterial on a structured beam," *Phys. Rev. X* **9**, 011040 (2019).
⁵A. Merkel, V. Romero-García, J.-P. Groby, J. Li, and J. Christensen, "Unidirectional zero sonic reflection in passive \mathcal{PT} -symmetric Willis media," *Phys. Rev. B* **98**, 201102 (2018).
⁶J. Li, C. Shen, A. Díaz-Rubio, S. Tretyakov, and S. Cummer, "Systematic design and experimental demonstration of bianisotropic metasurfaces for scattering-free manipulation of acoustic wavefronts," *Nat. Commun.* **9**, 1342 (2018).
⁷L. Quan, D. L. Sounas, and A. Alù, "Nonreciprocal Willis coupling in zero-index moving media," *Phys. Rev. Lett.* **123**, 064301 (2019).

⁸Y. Zhai, H.-S. Kwon, and B.-I. Popa, "Active Willis metamaterials for ultracompact nonreciprocal linear acoustic devices," *Phys. Rev. B* **99**, 220301 (2019).
⁹C. Olivier, G. Poignand, M. Malléjac, V. Romero-García, G. Penelet, A. Merkel, D. Torrent, J. Li, J. Christensen, and J.-P. Groby, "Nonreciprocal and even Willis couplings in periodic thermoacoustic amplifiers," *Phys. Rev. B* **104**, 184109 (2021).
¹⁰C. F. Sieck, A. Alù, and M. R. Haberman, "Origins of Willis coupling and acoustic bianisotropy in acoustic metamaterials through source-driven homogenization," *Phys. Rev. B* **96**, 104303 (2017).
¹¹M.-F. Ponge and P. O. D. Torrent, "Dynamic homogenization theory for nonlocal acoustic metamaterials," *Extreme Mech. Lett.* **12**, 71–76 (2017).
¹²A. L. Shuvalov, A. A. Kutsenko, A. N. Norris, and O. Poncelet, "Effective Willis constitutive equations for periodically stratified anisotropic elastic media," *Proc. R. Soc. A* **467**, 1749–1769 (2011).
¹³S. Nemat-Nasser, J. R. Willis, A. Srivastava, and A. V. Amirkhizi, "Homogenization of periodic elastic composites and locally resonant sonic materials," *Phys. Rev. B* **83**, 104103 (2011).
¹⁴A. Melnikov, Y. K. Chiang, Q. Li, S. Oberst, A. Alù, S. Marburg, and D. Powell, "Acoustic meta-atom with experimentally verified maximum Willis coupling," *Nat. Commun.* **10**, 3148 (2019).
¹⁵J.-P. Groby, M. Malléjac, A. Merkel, V. Romero-García, V. Tournat, D. Torrent, and J. Li, "Analytical modeling of one-dimensional resonant asymmetric and reciprocal acoustic structures as Willis materials," *New J. Phys.* **23**, 053020 (2021).
¹⁶L. Campos, "Some general properties of the exact acoustic fields in horns and baffles," *J. Sound Vib.* **95**, 177–201 (1984).
¹⁷V. Pagneux, N. Amir, and J. Kergomard, "A study of wave propagation in varying cross-section waveguides by modal decomposition. Part I. Theory and validation," *J. Acoust. Soc. Am.* **100**, 2034–2048 (1996).
¹⁸J. C. Samuels, "On propagation of waves in slightly rough ducts," *J. Acoust. Soc. Am.* **31**, 319–325 (1959).
¹⁹J. Golliard, Y. Aurégan, and T. Humbert, "Experimental study of plane wave propagation in a corrugated pipe: Linear regime of acoustic-flow interaction," *J. Sound Vib.* **472**, 115158 (2020).
²⁰L. Beranek and T. Mellow, *Acoustics: Sound Fields, Transducers and Vibration*, 2nd ed. (Academic Press, San Diego, CA, 2019).
²¹M. Červenka and M. Bednařík, "Acoustic bandpass filters employing shaped resonators," *J. Sound Vib.* **383**, 76–88 (2016).
²²A. Chaigne and J. Kergomard, *Acoustics of Musical Instruments, Modern Acoustics and Signal Processing*, 1st ed. (Springer, New York, 2016).
²³E. Eisner, "Complete solutions of the 'Webster' horn equation," *J. Acoust. Soc. Am.* **41**, 1126–1146 (1967).
²⁴S. W. Rienstra, "Webster's horn equation revisited," *SIAM J. Appl. Math.* **65**, 1981–2004 (2005).
²⁵O. V. Rudenko and A. B. Shvartsburg, "Nonlinear and linear wave phenomena in narrow pipes," *Acoust. Phys.* **56**, 429–434 (2010).
²⁶M. Bednařík and M. Červenka, "A wide class of analytical solutions of the webster equation," *J. Sound Vib.* **469**, 115169 (2020).
²⁷P. Honzík, S. Durand, N. Joly, and M. Bruneau, "On the acoustic transfer function of slowly tapered small horns filled with thermo-viscous fluid," *Acta Acust. united Acust.* **99**, 694–702 (2013).
²⁸M. Malléjac, T. Cavalieri, V. Romero-García, A. Merkel, D. Torrent, J. Christensen, J. Li, and J.-P. Groby, "Non-locality of the Willis coupling in fluid laminates," *Wave Motion* **110**, 102892 (2022).
²⁹M. R. Stinson, "The propagation of plane sound waves in narrow and wide circular tubes, and generalization to uniform tubes of arbitrary cross-sectional shape," *J. Acoust. Soc. Am.* **89**, 550–558 (1991).
³⁰W. P. Su, J. R. Schrieffer, and A. J. Heeger, "Solitons in polyacetylene," *Phys. Rev. Lett.* **42**, 1698–1701 (1979).
³¹A. Coutant, A. Sivadon, L. Zheng, V. Achilleos, O. Richoux, G. Theocharis, and V. Pagneux, "Acoustic Su-Schrieffer-Heeger lattice: Direct mapping of acoustic waveguides to the Su-Schrieffer-Heeger model," *Phys. Rev. B* **103**, 224309 (2021).